Real-time full-field characterization of transient dissipative soliton dynamics in a mode-locked laser

Piotr Ryczkowski, M. Närhi, Cyril Billet, Jean-Marc Merolla, Goëry Genty, John Michaël Dudley

Real-time full field measurements reveal transient dissipative soliton dynamics in a mode-locked laser

P. Ryczkowski[1†], M. Närhi[1†], C. Billet[2†], J.-M. Merolla[2], G. Genty[1], J. M. Dudley[2*]

1 Laboratory of Photonics, Tampere University of Technology, Tampere, Finland.

2 Institut FEMTO-ST, UMR 6174 CNRS-Université Bourgogne Franche-Comté, Besançon, France.

† Equal contributions

* Corresponding author john.dudley@univ-fcomte.fr

Dissipative solitons are remarkably localized states of a physical system that arise from the dynamical balance between nonlinearity, dispersion and environmental energy exchange. They are the most universal form of soliton that can exist, and are seen in far-from-equilibrium systems in many fields including chemistry, biology, and physics. There has been particular interest in studying their properties in mode-locked lasers, but experiments have been limited by the inability to track the dynamical soliton evolution in real-time. Here, we use simultaneous dispersive Fourier transform and time lens measurements to completely characterize the spectral and temporal evolution of ultrashort dissipative solitons as their dynamics pass through a transient unstable regime with complex break-up and collisions before stabilization. Further insight is obtained from reconstruction of the soliton amplitude and phase and calculation of the corresponding complex-valued eigenvalue spectrum. These findings show how real-time measurements provide new perspectives into ultrafast transient dynamics in optics.

INTRODUCTION

When operating in their steady-state regime, mode-locked lasers produce highly stable pulse trains which have found widespread applications in photonics and many other areas of science (*1-3*). However, mode-locked lasers can also exhibit complex instabilities when detuned from steady-state, or as stable mode-locking develops from noise (*4-6*). These instabilities are of particular interest in passively mode-locked fibre lasers, since they reveal a rich landscape of *dissipative soliton* dynamics (*7-10*). Dissipative solitons are the most universal class of localized soliton state in physics, existing for an extended period of time in the presence of nonlinearity and dispersion, even while parts of the structure can experience gain and loss (7). Although there is an extensive theoretical literature on fibre laser dissipative solitons, experiments have been more limited, and often restricted to measurements using only fast photodetectors (*6,9,11-13*). These experiments have certainly provided insight into the laser operation, but the limited available detector resolution has generally precluded detailed characterisation of the underlying dynamics.

Recent years, however, have seen dramatic advances in the real-time measurement of non-repetitive optical signals (*14-25*). The first method to see widespread use was the dispersive Fourier transform (DFT) which has yielded real-time spectral measurements of optical fibre rogue waves, modulation instability and supercontinuum generation (*14-18)*. More recently, the DFT has been applied to study the spectral properties of mode-locked lasers, revealing novel decoherence and soliton explosions in a fibre laser (*19,20*), and wavelength evolution dynamics in a Kerr-lens Ti:Sapphire laser (*21*). In addition, soliton dynamics in the Kerr-lens Ti:Sapphire laser have also been studied using a modified DFT adapted for real-time spectral interferometry (*22*). In parallel with these spectral measurements, the development of a temporal analogue of a spatial thin lens has resulted in real-time pulse intensity measurements with sub-picosecond resolution (*23*). This time-lens technique has been used in studies of incoherent soliton propagation in optical turbulence (*24*), and stochastic breather emergence in modulation instability (*25*).

In this work, we report the first simultaneous combination of real-time spectral DFT and time lens techniques to characterise unstable transient evolution characteristics of dissipative solitons in a mode-locked fibre laser. Our measurements provide a unified snapshot of how solitons evolve from round trip to round trip in the laser cavity, and allow the complex time and frequency domain characteristics of the evolving pulses to be directly correlated. One particular finding is the observation of transient coherent multi-soliton states, a previously experimentally-unobserved feature of soliton fibre lasers associated with short-lived soliton molecules that grow from noise and rapidly decay. In addition, phase retrieval allows reconstruction of the full field (intensity and phase) of the measured pulses and calculation of the corresponding complex nonlinear eigenvalue spectrum. These results provide a unique picture of the internal evolution of dissipative solitons, and we anticipate the wide application of our approach in the optimization and design of lasers with improved stability characteristics. More generally, we believe that our results will stimulate the widespread use of simultaneous temporal and spectral characterization as a standard technique for the real time study of ultrafast optical systems.

RESULTS

Our experiments studied the transient turn-on dynamics of a saturable absorber mode-locked fibre laser configured (in stable operation) to generate pulses of ~4.5 ps duration at 1545 nm with 20 MHz repetition rate (i.e. cavity round trip time of 50 ns). The laser cavity has net anomalous dispersion and in steady-state operation, frequency-resolved optical gating measurements confirmed that the stable output pulses were well-fitted by a hyperbolic secant profile and were transform limited with a uniform temporal phase (*26*). We used a commercial laser system in our experiments to highlight the practical utility of this technique in source development, and we selected the laser turn on phase as a readily-accessible regime that displays rich dynamics.

We characterized the turn-on dynamics using both direct photodiode detection as well as simultaneous DFT and time-lens measurements (see Methods for full details). Figure 1 shows results using direct photodiode detection. Specifically, Fig. 1(a) plots the envelope of the pulses

measured with reduced detection bandwidth to capture a time-window of 130 ms, corresponding to 2.6 million cavity round trips. The figure clearly reveals a ~100 ms transient regime of Q-switched mode-locked operation before the appearance of a stable pulse train. Figure 1(b) shows a separate measurement of a portion of the transient regime as indicated, but here using 30 GHz detection bandwidth so that it is possible to resolve a series of ~10 μs bursts separated by a ~70 μs period. The expanded view in Fig. 1(b) shows how under each burst, an irregular train of mode-locked pulses (at 50 ns period) is present. In contrast with this unstable regime, Fig. 1(c) shows measurements in the stable mode-locked regime using 30 GHz detection, to illustrate a regular pulse train of constant intensity. Of course, such complex transient dynamics have been seen in both numerical and experimental studies of a range of other passively-mode-locked lasers (*27-34*), but we include these measurements here for completeness. The key point is that, even with a detection bandwidth of 30 GHz, the temporal width of the pulses seen in the photodiode intensity record is ~30 ps, precluding any detailed study of the underlying soliton dynamics in the transient regime. It is this limitation that we overcome with our simultaneous real-time DFT and time-lens measurements.

Figure 2 shows the setup used. Light from the fibre laser output was split into two paths and sent to the real-time DFT and time-lens acquisition arms. Real time spectral measurements used a standard DFT set up (*18*) with spectral resolution of ~0.3 nm. The time lens set-up was similar to that described in Ref. (*25*) and was capable of real-time measurements of intensity profiles spanning a temporal window up to 60 ps duration and with an effective temporal resolution of 400 fs. Both DFT and time lens signals were recorded using a high storage capacity digital oscilloscope, with data acquisition triggered by the time-lens signal detected after the laser was turned on. We could simultaneously measure spectral and temporal intensity profiles over a maximum of 400 cavity roundtrips (see Methods).

We recorded multiple data sequence to examine the spectral and temporal soliton dynamics both in the Q-switched mode-locked and the stable-modelocking regime. We begin in Fig. 3(a) by showing results for the stable modelocking regime where as expected the (i) spectral,

and (ii) temporal intensity profiles are constant with roundtrip. The extracted spectral and temporal widths and the integrated pulse energy are shown as the right subfigures; the small (noise) variations in these figures is of the order of the experimental resolution of the spectral and temporal measurements.

Although the ability to measure both temporal and spectral intensity in real time is itself a highly significant advance, we extend this technique further using Gerchberg-Saxton phase-retrieval (*35*,*36*) to recover the corresponding complex electric field of each pulse (see Methods). These results are shown in Fig. 3(a-iii) where we plot the retrieved intensity (left axis) and phase (right axis) revealing the soliton characteristics of near-uniform phase. Access to the full complex electric field allows us to calculate the associated wavelength-time spectrogram (see Methods), and these results are shown in Fig. 3(a-iv), confirming the localized soliton-like nature of the pulses. Fig 4 shows similar results, but from a data sequence just prior to the regime of stable modelocking. Here, over a relatively small number of round trips, we see significant modulation in both the measured spectral and temporal amplitudes, as well as energy variation of ~30%. This "breathing" of the intracavity pulses just prior to the onset of stability is a known property of dissipative soliton dynamics in mode-locked lasers (*21*), but our results are the first to be able to experimentally characterize it completely in both the time and frequency domains.

Dissipative solitons can display a much richer range of interaction dynamics (*7*-*9*), and Fig. 4 shows examples of this behaviour in the evolution of pulses under a transient Q-switched burst. To capture different aspects of these dynamics, we repeated experiments restarting the laser many times, using a variable hold off time for our measurement window to scan various points of the transient regime (see Methods). In fact, we found that whilst the general dynamics were similar for all burst durations (i.e. showing the emergence of multiple pulses from noise followed by subsequent decay) the detailed evolution dynamics varied significantly for different bursts. Indeed, our measurement set-up allowed us to reveal previously unobserved regimes of dissipative soliton propagation and interaction under the transient envelope.

Remarking firstly that the spectral and temporal evolution with round trip is plotted from top to bottom, two typical results are shown in Fig. 4(a) and 4(b) to illustrate the different types of behaviour observed. The figures show (i) spectral and (ii) temporal intensity profiles (with the right subfigure showing energy), as well as (iii) retrieved intensity and phase, and (iv) spectrograms. Also note that energy is not constant in this transient turn-on regime (*12*). We first discuss Fig. 4(a) which shows an initial noisy field splitting into 3 distinct pulses (of duration ~5 ps) that propagate coherently together over ~100 roundtrips. Each pulse displays a well-localized temporal intensity peak, and the pulses are mutually coherent as shown by the distinct modulation in the corresponding spectrum. Significantly, the pulse separation does not vary over ~100 roundtrips as the pulses evolve without seeming to interact before decaying. Figure 4(b) shows a qualitatively different case. Here, two pulses emerge, but rather than propagating without interacting, they undergo attraction and eventually collide, displaying a more complex nonlinear phase profile at this point. Figure 4(c) on the other hand shows another example of burst evolution where a combination of the above dynamics are observed with the emergence of 3 solitons.

From analysis of multiple Q-switched bursts, we have been able to identify that the emergence of multi-pulse states consisting of 2 or 3 distinct soliton-like structures is a typical feature of this transient regime. Such bound coherent soliton states in a laser are referred to as soliton molecules, and are well-known to exhibit a rich range of dynamical behaviour (*37*). Significantly, in contrast to previous studies of stable or periodic dynamics characterized using spectral measurements (*22,38*), our results reveal both time and frequency domain signatures of a regime of short-lived growth and decay that has not previously been observed experimentally. We also note that the interaction dynamics between the pulses within the soliton molecule can be very complex, depending on the pulse frequencies, their temporal separation, as well as their initial amplitudes and phases (*37, 39-42*). In this context, the spectrogram plots in Fig. 4 are useful in illustrating this complexity. In Fig. 4(a) for example, the central frequencies of the constituent pulses change very little with propagation, whereas in Fig 4(b-c) the two pulses that eventually

merge initially display a frequency difference of 0.4 and 0.5 nm, respectively, but their frequencies evolve with propagation until they eventually coincide at their superposition.

The ability to completely reconstruct the complex electric field from the measured pulse intensity and phase allows calculation of derived quantities that yield additional and important physical insights. In particular, it is possible to apply numerical techniques from scattering theory to yield spectral eigenvalue portraits of the pulse structures (*43-47*). More specifically, according to inverse scattering theory, any initial condition of the nonlinear Schrödinger equation (NLSE) evolves into a combination of solitons plus non-solitonic (quasi nonlinear) oscillating wave packets, and it is the parameters of the solitons formed that is derived via the inverse scattering transform (*47*). Interestingly, although inverse scattering in fibre optics has generally been used only analytically to obtain closed form solutions to the NLSE, there has also been recent interest in using numerical techniques (often described as a nonlinear Fourier transform) for more arbitrary fields to study rogue wave dynamics (*48*) and to overcome channel limits in optical communications (*49*).

With this approach applied to the intensity and phase measurements of pulses from the modelocked fibre laser, the calculated eigenspectra for several cases are shown in Fig. 5. Here the red dots in each subfigure show the discrete eigenspectrum for the normalized pulse intensity profiles shown as insets. Here ψ is the normalised pulse envelope that generates the scattering potential, τ is the time variable, and ζ is the calculated eigenvalue (see Methods). In this case, we associate the stable pulse regime in Fig. 3(a) with solitons having eigenvalues at $\zeta = \pm 0.5i$ in the complex plane, physically equivalent to injecting them in optical fibre with initial conditions corresponding to a fundamental soliton. Based on the measurements in Fig. 3(a), we normalize the intensities of other measured pulses with respect to these ideal solitons and perform direct scattering analysis to determine the corresponding more complex eigenvalue spectrum (see Methods and also the Supplementary Information).

We first consider the results in Fig. 5 (a) and (b) which correspond to single pulses at two points of the breather cycle shown in Fig. 3(b-iii). In each case the scattering analysis yields one distinct eigenvalue, and we see that as the pulse intensity varies below and above the unity value of a normalized fundamental soliton (dashed black line), the eigenvalue Im(ζ) also varies below and above the ideal soliton value of ±0.5*i*. In other words, the variation in the eigenvalue reflects the breathing of the pulse properties in this regime. We also note the residual "eye-like" structure in the eigenvalue spectrum corresponding to the small pedestal in the intensity distribution (see also Supplementary Information).

Figure 5(c) and (d) consider more complex evolution. Figure 5(c) plots the eigenvalue spectrum for the double-soliton pulse shown in Fig. 4(b-iii) where the direct scattering procedure yields two discrete eigenvalues, both with Im(ζ) ~ ±0.5*i*. Figure 5 (d) shows results for the three-soliton case in Fig. 4(a) and here we see two discrete eigenvalues with Im(ζ)~±0.5*i* and a third eigenvalue at a slightly lower value. As in the breathing regime of Fig. 3(b) we note the presence of a residual pedestal manifested around the zero of the real axis in the nonlinear spectrum. In all cases, the clear separation of the eigenvalues from the real axis indicates that this particular dynamical regime within the laser bursts prior to steady-state modelocking can be considered as creating discrete pulse complexes, similar to those seen with multiple bound solitons (*7-9*). This is a very important physical insight that the nonlinear Fourier transform reveals directly.

DISCUSSION

Dissipative nonlinear systems can be highly complex, but it is clear that recent years have seen tremendous advances in being able to understand their behavior through novel theoretical approaches and numerical modelling. Of course, a full understanding of such complex dynamical phenomena requires that theoretical and numerical results are carefully compared with experiment, and to this end the measurement technique and phase retrieval analysis reported in this paper make a significant contribution in enabling complete characterization of picosecond dissipative soliton systems. The results obtained show a range of ultrafast temporal and spectral

dynamics, and in particular we have shown temporal and spectral measurements of a transient phase of soliton dynamics associated with the emergence and decay of coherent multi-soliton states. We anticipate that our results will stimulate many future theoretical studies and numerical modelling to understand the underlying pulse dynamics, building on the extensive existing literature (*37*) and including also possible long-range interactions arising from transverse acoustic waves generated through soliton-induced electrostriction (*50*).

More generally, these results also highlight the novelty of the simultaneous use of time-lens and DFT measurement technique in providing real-time pulse ultrafast pulse measurements that can yield complete intensity and phase characterisation. When compared to other full field techniques measurement techniques such as Frequency-Resolved Optical Gating *(36)* or Spectral Phase Interferometry for Direct Electric-field Reconstruction *(51)*, simultaneous time-lens and DFT measurements operate at orders of magnitude lower peak power (typically ~1 W peak power is required by the time lens, < 100 mW peak power by the DFT). Moreover, acquisition is possible at the 20 MHz repetition rate of the laser and with asynchronous operation of the time-lens, can be extended to GHz repetition rates. To our knowledge, no other technique can be used to provide real-time characterisation and intensity and phase information of ultrafast instabilities such as those reported here. The temporal resolution in our setup is ultimately limited by the phase matching properties of the silicon waveguide and the duration of the pump pulse in the time-lens system, but resolutions in the ~200 fs range have been reported *(52)* and further improvement might be expected with dedicated waveguide dispersion-engineering.

A further area of particular significance concerns our use of the nonlinear Fourier transform to calculate the local eigenspectrum of the pulses generated from the modelocked fibre laser. The calculated spectra clearly show the presence of local soliton content in the complex pulse profiles measured, which provides a new window into the physics of the underlying laser dynamics. We also believe our results will motivate interest in much broader applications of the nonlinear Fourier transform for characterising soliton content of ultrashort pulses (*53,54)*. In optics, we anticipate particular interest in real-time spectral and temporal studies of nonlinear

single-pass propagation dynamics in optical fibres such as rogue wave and modulation instability that also display complex transient noise spikes.

METHODS

Experimental Setup

The fibre laser used in our experiments was a commercial Pritel FFL-500 model using a linear Fabry-Perot cavity configuration shown in Fig. 2, similar to that described in (*55*) but with a 978 nm pump laser and Er:doped fibre gain medium. Modelocking is sustained by a 2 μm thick bulk saturable absorber (InGaAs on InP substrate) contact bonded to one of the cavity mirrors. The steady-state modelocking dynamics are dominated by soliton propagation effects because of the net anomalous dispersion in the cavity, with the generation of hyperbolic-secant like pulses of flat phase in stable operation.

We implemented the DFT technique using 850 m of dispersion compensating fibre (DCF) with group velocity dispersion coefficient of 100 ps/nm.km and dispersion slope 0.33 ps/nm^2.km at 1550 nm. We attenuated the input to the DCF in order to ensure linear propagation, and confirmed the fidelity of the time-stretching technique when the fibre laser was operated in the stable mode-locked regime by comparing the DFT spectrum with that measured using an optical spectrum analyser (Anritsu MS9710B). The real-time DFT signal was measured by a 35 GHz photodiode (New Focus 1474 A) connected to a 30 GHz channel of a real-time oscilloscope (LeCroy 845 Zi-A, 80 GS/s), resulting in a spectral resolution of 0.3 nm.

The time lens measurements used a commercial Picoluz UTM-1500 system described previously in (*24*) with a temporal magnification factor of 76.4. Total accumulated dispersion for the input and output propagation steps was: D_1 = 4.16 ps/nm and D_2 = 318 ps/nm respectively, with magnification $|M| = D_2/D_1$. The temporal quadratic phase (to reproduce the effect of a thin lens) was imposed through four wave mixing from a pump pulse (100 MHz Menlo C-Fiber Sync and P100-EDFA) with linear chirp accumulated from propagation in a pre-chirping fibre D_p. The imaging condition for magnification is $2/D_p = 1/D_1 + 1/D_2$ so that the dispersion for the pump is around twice that of the signal input step. The signal at the time lens output is recorded by a 13 GHz photodiode (Miteq 135GE) connected to the 30 GHz channel of the real-time oscilloscope

at a sampling rate of 80 Gs/s, resulting in an effective 400 fs temporal resolution over a (demagnified) time window of 60 ps. The temporal window is determined by the pump pulse duration used in the time lens to impose the required quadratic chirp via four-wave mixing in a highly nonlinear Si waveguide (*52*). In stable mode-locked operation it is possible to synchronize the 20 MHz laser under study with the 100 MHz pump laser, but this is not the case when studying the transient dynamics as there is significant amplitude and phase noise that precludes the detection of a well-defined 20 MHz harmonic for repetition-rate locking. The time lens is therefore operated in asynchronous mode with free-running acquisition triggered by the arrival of the time lens signal, although this limits the number of roundtrips that can be simultaneously measured to ~400 (as there is a walk-off between the Q-switched mode-locked pulses relative to the time lens gate).

To obtain representative data sets at different times of the transient regime evolution we performed multiple measurements with different delays between the switch-on time of the fibre laser and the time lens trigger, restarting the laser between each measurement. We can use this approach to characterize different phases of the pulse evolution in the transient regime because: (i) the measurement window of 400 roundtrips (20 μs) is longer than that of the typical transient bursts that have lifetimes of only 200-300 roundtrips (10-15 μs), and (ii) we can use a variable hold-off trigger for different measurements and thus capture different phases of the overall transition phase that lasts over many millions of round trips (~100 ms). Although the recorded time window precludes the real-time measurement of the full 100 ms transient regime with sub-ps resolution, this technique allows recording of many key dynamical features. We also emphasize that we performed many hundreds of measurements under conditions of different laser restarts to study different phases of the laser dynamics and obtained consistently results similar to those in Fig. 3(b) (breathing) and Fig. 4 (multiple pulse behaviour).

In more detail, the triggering scheme used was as follows. We employed a two-stage triggering scheme in the ultrafast oscilloscope with an adjustable hold-off time between the two trigger signals. The first trigger was obtained from the first measured DFT pulse (i.e. the first Q-

switched mode-locked burst in the full transient evolution cycle) which starts the hold-off countdown time. Once the hold-off time has passed, the actual acquisition of the temporal profile is triggered from the first signal at the time lens output. By performing repeated measurements for different laser restarts with varying hold-off times in the range (1-100 ms), we could readily examine the dynamical properties of bursts throughout the full transition regime.

Finally, we note that because the optical path lengths of the DFT and time lens steps were different, the delay between time-lens and DFT records was calibrated (in a separate measurement) by comparing the arrival times on the oscilloscope of a characteristic intensity pattern imprinted onto a CW laser. This allowed us to match without ambiguity the real-time temporal and spectral intensity profiles of the dissipative solitons during their transient evolution phase.

Phase Retrieval

Phase retrieval was performed with the Gerchberg-Saxton algorithm (*35*). Aside from a few trivial ambiguities, this algorithm is known to be accurate for pulse retrieval when intensity envelopes are measured both in the spectral and time domains. The algorithm constructs an initial guess for the profile of the electric field using the measured temporal intensity $I_M(t)$ and an initial random phase $\phi_{\text{rand}}(t)$: $E_g(t) = \sqrt{I_M(t)}\, e^{i\phi_{\text{rand}}(t)}$ which is then Fourier transformed to the spectral domain to yield a corresponding initial guess for the spectral amplitude and phase FT $[E_g(t)] = \sqrt{S(\omega)}e^{i\varphi(\omega)}$. The next step involves retaining the calculated spectral phase but replacing the calculated spectral amplitude with the measured spectral amplitude i.e. $\sqrt{S_M(\omega)}e^{i\varphi(\omega)}$. This updated spectral profile is then transformed back into the time domain where we retain the calculated temporal phase but again replace the calculated amplitude with that from experiment $\sqrt{I_M(t)}$. This procedure is iteratively repeated until the root mean square error between the measurements and retrieved intensity profiles becomes smaller than a chosen value

(3×10^{-5} in our case). Convergence was improved by applying the measured temporal and spectral constraints only where the measured intensities were well above the noise floor (-20 dB from the maximum). Elsewhere the amplitudes were multiplied with a small constant value of 0.001 forcing them below the noise. If the algorithm was detected to stagnate (no change in the retrieval error before reaching the desired value), a small additional random phase contribution was added. The reliability of the algorithm was tested with simulated pulses with complex properties similar to those seen in experiments, and by performing multiple retrievals on the same experimental data, which all converged to the same results (within the retrieval error). Examples of retrievals using numerical data and additional information can be found in the Supplementary Information.

Spectrogram Calculation

Access to the full field in amplitude and phase allows us to calculate a frequency (or wavelength)-time spectrogram. For a pulse with complex field $E(t)$, the spectrogram can be interpreted as the modulus squared of a short-time Fourier transform, a function that represents the intensity and phase content of the pulse in the time and frequency domains simultaneously. The spectrogram is defined by:

$$S(\omega,\tau) = \left| \int_{-\infty}^{\infty} E(t) g(t-\tau) e^{-i\omega t} dt \right|^2 , \qquad (1)$$

with $g(t-\tau)$ a variable delay gate function with delay value τ. The spectrogram thus shows the spectra of a series of time-gated portions of $E(t)$ and provides a highly intuitive and visual means of interpreting the frequency-time content of a complex field. In our calculation of the spectrograms from experimental data, we used a Gaussian pulse gate function of duration (full width at half maximum) of 4 ps.

Nonlinear Fourier Transform

The nonlinear Fourier transform (also known as the direct scattering transform) is a mathematical procedure that identifies and quantifies soliton content in a given pulse structure. In fact, any initial condition of the NLSE evolves into a combination of solitons plus quasilinear oscillating wave packets and it is the scattering transform that can be used to determine the number of solitons formed as well as their associated parameters. In particular, we consider a system described by the NLSE in normalised form:

$$i\frac{\partial \psi}{\partial \xi}+\frac{1}{2}\frac{\partial^2 \psi}{\partial \tau^2}+|\psi|^2\psi=0 \tag{2}$$

where ψ is the normalised pulse envelope that generates the scattering potential, ξ is the propagation variable and τ is the time variable in a co-moving frame. The associated scattering problem yields the following system (*42*):

$$\begin{aligned}\frac{\partial v_1}{\partial \tau}+\psi v_2&=\zeta v_1\\ \frac{\partial v_2}{\partial \tau}+\psi^* v_1&=-\zeta v_2\end{aligned} \tag{3}$$

where v_1 and v_2 are the amplitudes of the waves scattered by the potential induced by ψ, and ζ is the corresponding complex eigenvalue. For our results, we consider the laser output pulses in stable operation Fig. 3(a) as associated with solitons having eigenvalues at $\zeta = \pm 0.5i$ in the complex plane. This would be physically equivalent to injecting them in optical fibre with initial conditions corresponding to a fundamental soliton, obtained for example by appropriate adjustment of the injected power. This case corresponds to amplitude $|\psi| = 1$, and the field profiles corresponding to the other pulses analysed were normalised relative to this value. Standard numerical techniques (matrix methods) were used to determine the eigenvalue spectrum (*56)*.

ACKNOWLEDGEMENTS

Funding

This work was supported by the Agence Nationale de la Recherche project LABEX ACTION ANR11-LABX-0001-01, the Region of Franche-Comté Project CORPS and the Academy of Finland (Grants 267576 and 298463).

Contributions

All authors participated in all the experimental work and data analysis reported, and in the writing and review of the final manuscript. G.G. and J.M.D. planned the research project and provided overall supervision. The authors also thank K. V. Reddy for providing technical details concerning the soliton operating regime of the Pritel laser used in these experiments.

Competing financial interests

The authors declare no competing financial interests.

Corresponding authors

Correspondence to: John M. Dudley

REFERENCES

1. French, P. M. W. The generation of ultrashort laser pulses, *Rep. Prog. Phys.* **58,** 169-267 (1995).
2. Keller, U. Recent developments in compact ultrafast lasers, *Nature* **424**, 831-838 (2003).
3. Hänsch, T. W. Nobel Lecture: Passion for precision, *Rev. Mod. Phys.* **78**, 1297-1309 (2006).
4. Abraham, D., Nagar, R., Mikhelashvili, V. & Eisenstein, G. Transient dynamics in a self-starting passively mode-locked fiber-based soliton laser, *Appl. Phys. Lett.* **63**, 2857-2859 (1993).
5. Dudley, J. M., Loh, C. M. & Harvey, J. D. Stable and unstable operation of a mode-locked argon laser, *Quantum Semiclass. Opt.* **8** 1029-1039 (1996).
6. Hönninger, C., Paschotta, R., Morier-Genoud, F., Moser, M. & Keller, U. Q-switching stability limits of continuous wave passive mode locking, *J. Opt. Soc. Am. B* **16**, 46-56 (1999).
7. Akhmediev, N. & Ankiewicz, A. (Eds.), *Dissipative Solitons.* Lecture Notes in Physics, Springer-Verlag, 2005.
8. Grelu, P. & Akhmediev, N. Dissipative solitons for mode-locked lasers, *Nat. Photon.* **6**, 84–92 (2012).
9. Grelu, P. (Ed.) *Nonlinear Optical Cavity Dynamics: From Microresonators to Fiber Lasers.* Wiley, 2016.
10. Turitsyn, S. K. *et al.* Dissipative solitons in fiber lasers, *Phys. Usp.* **59**, 642-668 (2016).
11. Flynn, M. B., O'Faolain, L. & Krauss, T. F. An experimental and numerical study of Q-switched mode-locking in monolithic semiconductor diode lasers, *IEEE J. Quant. Electron.* **40**, 1008-1013 (2004).
12. Schlatter, A., Zeller, S. C., Grange, R., Paschotta, R. & Keller, U. Pulse-energy dynamics of passively mode-locked solid-state lasers above the Q-switching threshold, *J. Opt. Soc. Am. B* **21**, 1469-1478 (2004).
13. Lecaplain, C., Grelu, P., Soto-Crespo, J. M. & Akhmediev, N. Dissipative rogue waves generated by chaotic pulse bunching in a mode-locked laser, *Phys. Rev. Lett.* **108**, 233901 (2012).

14. Goda, K. & Jalali, B. Dispersive Fourier transformation for fast continuous single-shot measurements, *Nat. Photon.* **7**, 102-112 (2013).

15. Solli, D. R., Ropers, C., Koonath, P. & Jalali, B. Optical rogue waves, *Nature* **450,** 1054-1057, (2007).

16. Godin, T. *et al.* Real time noise and wavelength correlations in octave-spanning supercontinuum generation, *Opt. Exp.* **21**, 18452-18460 (2013).

17. Solli, D. R., Herink, G., Jalali, B. & Ropers, C. Fluctuations and correlations in modulation instability, *Nat. Photon.* **6**, 463-468 (2012).

18. Wetzel, B. *et al.* Real-time full bandwidth measurement of spectral noise in supercontinuum generation, *Sci. Rep.* **2**, 882 (2012).

19. Runge, A. F. J., Aguergaray, C., Broderick, N. G. R., Erkintalo, M. Coherence and shot-to-shot spectral fluctuations in noise-like ultrafast fiber lasers, *Opt. Lett.* **38**, 4327-4330 (2013).

20. Runge, A. F. J., Broderick, N. G. R. & Erkintalo, M. Observation of soliton explosions in a passively mode-locked fiber laser, *Optica* **2**, 36-39 (2015).

21. Herink, G., Jalali, B., Ropers, C. & Solli, D. R. Resolving the build-up of femtosecond mode-locking with single-shot spectroscopy at 90 MHz frame rate, *Nat. Photon.* **10**, 321–326 (2016).

22. Herink, G., Kurtz, F., Jalali, B., Solli, D. R. & Ropers, C. Real-time spectral interferometry probes the internal dynamics of femtosecond soliton molecules, *Science* **356**, 50–54 (2017).

23. Kolner B. H. & Nazarathy, M. Temporal imaging with a time lens, *Opt. Lett.* **14**, 630-632 (1989).

24. Suret, P. *et al.* Single-shot observation of optical rogue waves in integrable turbulence using time microscopy, *Nat. Commun.* **7**, 13136 (2016).

25. Närhi, M. *et al.* Real-time measurements of spontaneous breathers and rogue wave events in optical fibre modulation instability. *Nat. Commun.* **7**, 13675 (2016).

26. Billet, C., Dudley, J. M. ,Joly, N. & Knight, J. C. Intermediate asymptotic evolution and photonic bandgap fiber compression of optical similaritons around 1550 nm, Opt. Express **13**, 3236-3241 (2005).

27. Soto-Crespo, J. M., Akhmediev, N. & Town, G. Continuous-wave versus pulse regime in a passively mode-locked laser with a fast saturable absorber, *J. Opt. Soc. Am. B*. **19**, 234-242 (2002).

28. Schreiber, T., Ortaç, B., Limpert, J. & Tünnermann, A. On the study of pulse evolution in ultra-short pulse mode-locked fiber lasers by numerical simulations, *Opt. Express* **15**, 8252-8262 (2007).

29. Sarukura, N. & Ishida, Y. Pulse evolution dynamics of a femtosecond passively mode-locked Ti:sapphire laser, *Opt. Lett.* **17**, 61–63, (1992).

30. Vodonos B. *et al.*, Experimental study of the stochastic nature of the pulsation self-starting process in passive mode locking, *Opt. Lett.* **30**, 2787-2789 (2005).

31. Li, H., Ouzounov, D. G. & Wise, F. W. Starting dynamics of dissipative-soliton fiber laser, *Opt. Lett.* **35**, 2403-2405 (2010).

32. Zinkiewicz, Ł., Ozimek, F. & Wasylczyk, P. Witnessing the pulse birth-transient dynamics in a passively mode-locked femtosecond laser, *Laser Phys. Lett.* **10**, 125003, (2013).

33. Ghiu Lee, C., Kim, J., Kim, S. & Petropoulos, P. Transient response of a passively mode-locked Er-doped fiber ring laser, *Opt. Commun.* **356**, 161–165, (2015).

34. Wang, Z. *et al.*, Q-switched-like soliton bunches and noise-like pulses generation in a partially mode-locked fiber laser, *Opt. Express* **24**, 14709–14716, (2016).

35. Gerchberg R. W. & Saxton, W. O. A practical algorithm for the determination of the phase from image and diffraction plane pictures, *Optik* **35**, 237 (1972).

36. Trebino, R. *Frequency-Resolved Optical Gating: The Measurement of Ultrashort Laser Pulses*. Springer, 2000.

37. Grelu, P. & Soto-Crespo, J. M. Temporal Soliton "Molecules" in Mode-Locked Lasers: Collisions, Pulsations, and Vibrations. In: Dissipative Solitons: From Optics to Biology and Medicine. Lecture Notes in Physics, vol 751. Springer, Berlin, Heidelberg (2008)

38. Krupa, K., Nithyanandan, K., Andral, U., Tchofo-Dinda, P., Grelu, P. Real-Time Observation of Internal Motion within Ultrafast Dissipative Optical Soliton Molecules, *Phys. Rev. Lett*. **118**, 243901 (2017)

39. Tang, D. Y., Zhao, B., Zhao, L. M. & Tam, H. Y. Soliton interaction in a fiber ring laser, *Phys. Rev. E* **72**, 16616 (2005).

40. Roy, V., Olivier, M. & Piché, M. Pulse interactions in the stretched-pulse fiber laser, *Opt. Express* **13**, 9217-9223 (2005).

41. Akhmediev, N., Soto-Crespo, J. M., Grapinet, M. & Grelu, P. Dissipative soliton interactions inside a fiber laser cavity, *Opt. Fib. Tech.* **11**, 209-228 (2005).

42. Akhmediev, N., Soto-Crespo, J. M. & Town, G. Pulsating solitons, chaotic solitons, period doubling, and pulse coexistence in mode-locked lasers: complex Ginzburg-Landau equation approach., *Phys. Rev. E* **63**, 56602 (2001).

43. Zakharov V. E. & Shabat, A. B. Exact theory of two-dimensional self-focusing and one-dimensional self-modulation of waves in nonlinear media, *Sov. Phys. JETP* **34**, 62–69 (1972).

44. Akhmediev, N. & Ankiewicz, A. Solitons: Non-linear Pulses and Beams. Chapman & Hall, 1997.

45. Osborne, A. R. Nonlinear Ocean Waves and the Inverse Scattering Transform. Elsevier, 2010.

46. Agrawal, G. P. Nonlinear Fiber Optics, Elsevier, 2013.

47. Turitsyn, S. K. & Derevyanko, S. A. Soliton-based discriminator of noncoherent optical pulses. Phys. Rev. A **78**, 063819 (2008)

48. Randoux, S., Suret, P. & El, G. Inverse Scattering Transform Analysis of Rogue Waves Using Local Periodization Procedure, *Sci. Rep.* **6**, 29238 (2016).

49. Turitsyn, S. K. *et al.* Nonlinear Fourier transform for optical data processing and transmission: advances and perspectives, *Optica* **4**, 307-322 (2017).

50. Jang, J. K., Erkintalo, M., Murdoch, S. G., Coen, S. Ultraweak long-range interactions of solitons observed over astronomical distances. Nat. Photon. **7**, 657-663 (2013).

51. Iaconis, C, & Walmsley, I. A. Spectral phase interferometry for direct electric-field reconstruction of ultrashort optical pulses", *Opt. Lett.* **23**, 792-794 (1998).

52. Salem, R., Foster, M. A., Gaeta, A. L. Application of space-time duality to ultrahigh-speed optical signal processing. Adv. Opt. Photon. **5**, 274–317 (2013).

53. Sugavanam, S., Kamalian, M., Peng, J., Prilepsky, J. E. & Turitsyn, S. K. Experimentally Characterized Nonlinear Fourier Transform of a Mode-locked Fibre Laser, 2017 Conference on Lasers and Electro-Optics Europe & European Quantum Electronics Conference, paper EF-2.6 (2017).

54. Narhi, M., Ryczkowski, P., Billet, C., Genty, G. & Dudley, J. M. Ultrafast Simultaneous Real Time Spectral and Temporal Measurements of Fibre Laser Modelocking Dynamics, 2017 Conference on Lasers and Electro-Optics Europe & European Quantum Electronics Conference, paper EE-3.5 (2017).

55. Reddy, K. V. *et al.* A Turnkey 1.5 μm picosecond Er/Yb Fiber Laser, *Conference on Optical Fiber Communication (OFC)*, OSA Technical Digest Series, paper PD17 (1993).

56. Wahls, S. & Poor, H. V. Fast Numerical Nonlinear Fourier Transforms. IEEE Trans. Inf. Theory **6**, 6957- 6974 (2015).

Figure 1. **Direct photodetector measurement of transient laser dynamics.** (a) Results recorded with reduced bandwidth detection of 20 MHz illustrating the ~100 ms transient regime of Q-switched mode-locked operation before stable mode-locking. The total time record shown corresponds to 2.6 million round trips. (b) Results from separate measurements using 30 GHz bandwidth detection, showing how the laser output during the Q-switched mode-locked regime consists of transient bursts of temporal width ~10 μs separated by ~70 μs period. The expanded view shows how unstable mode-locked pulses at 50 ns period are generated under each burst. (c) Results using 30 GHz detection but in the stable mode-locked regime, showing a regular train of pulses with constant amplitude.

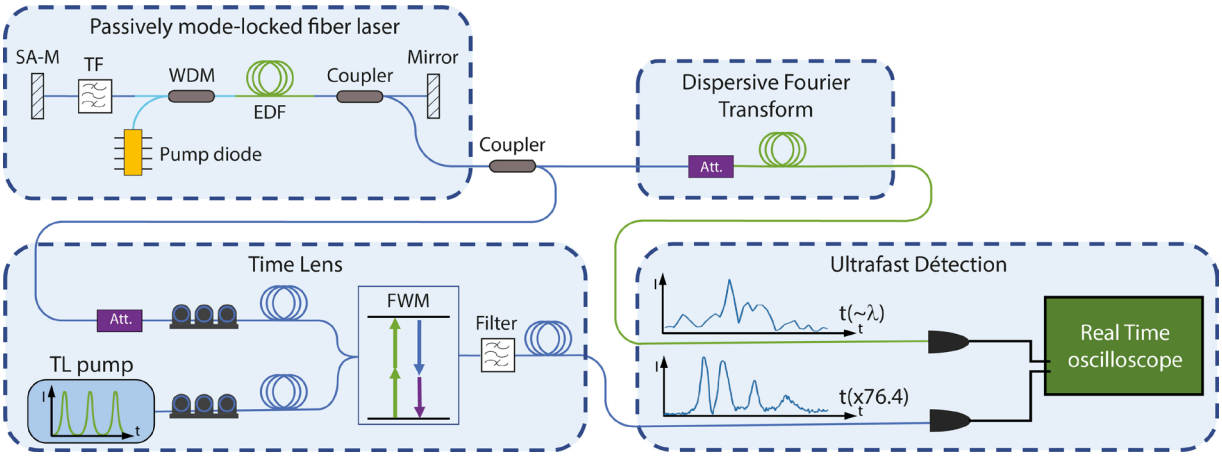

Figure 2. **Setup used for real-time characterization.** Pulses from a 20 MHz passively mode-locked fibre laser are split into two paths in a fibre coupler and sent to a DFT real time spectral setup and a time-lens. The DFT used 850 m of dispersion compensating fibre (DCF) to perform time to wavelength conversion, with detection using a 35 GHz bandwidth photodiode (PD_2). An optical spectrum analyzer was also used for control measurements of the spectrum. The time lens uses two dispersive propagation steps (D_1 and D_2), one on each side of a silicon waveguide stage that applies a quadratic temporal phase through four wave mixing (FWM) with linearly-chirped pump pulses generated from a 100 MHz femtosecond pulse fibre laser (TL Pump) after stretching in a dispersive stretching fibre D_p. The time lens signal is extracted from the FWM spectrum by an optical filter and was measured using a 13 GHz bandwidth photodiode (PD_1). Both PD_1 and PD_2 were input to a 30 GHz channel of the real-time oscilloscope. Values for dispersion modules D_1, D_2 and D_p in the time lens are given in Methods. The inputs to both the DFT and time lens were attenuated (Att.) to avoid nonlinear effects and polarization control (PC) was needed to ensure optimal signal from the time-lens. The passively modelocked laser was a commercial Pritel FFL-500 model which was based on a standing wave cavity with a saturable absorber mirror (SA-M) and a tunable spectral filter (TF) of 3dB bandwidth 2 nm (see also Methods).

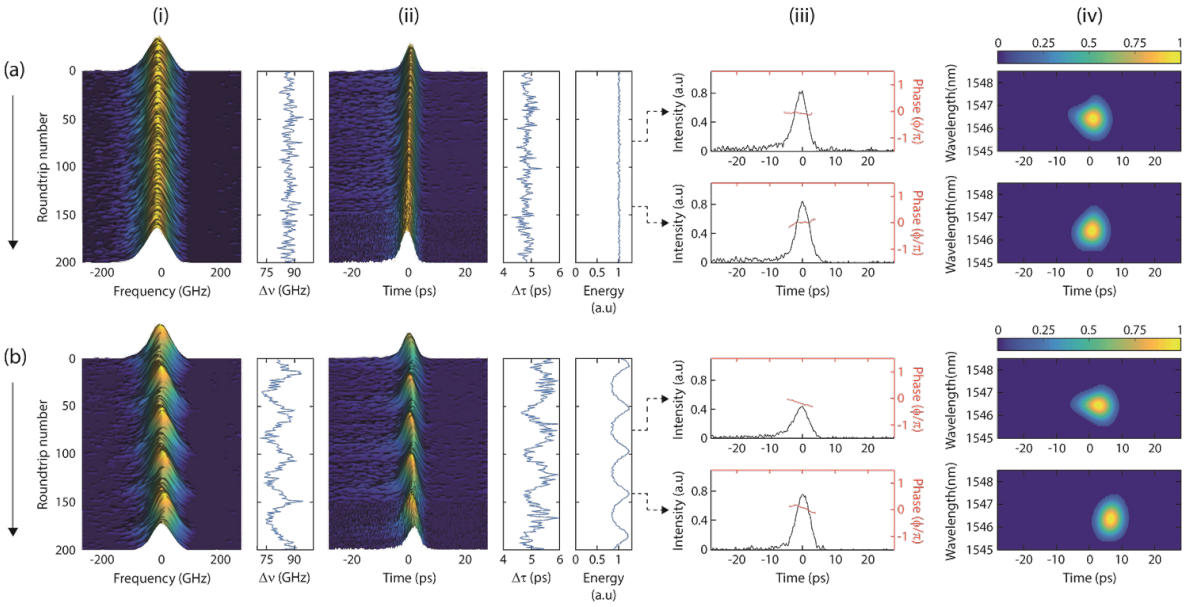

Figure 3. **Real-time spectral and temporal characterization near stability**. Results shown over 200 roundtrips for (a) stable and (b) breathing mode-locking regimes. (i) Measured spectral intensity with the extracted spectral width shown in the right subfigure. (ii) Measured temporal intensity with the extracted temporal width and energy shown in the right subfigures. (iii) Corresponding temporal intensity (left axis) and phase (right axis) extracted using the Gerchberg-Saxton algorithm for pulses at points indicated by arrows. For each of the extracted pulses in (iii), the plots in (iv) show the calculated wavelength-time spectrogram. The colour scale shows spectrogram intensity in linear arbitrary units normalised relative to the maximum.

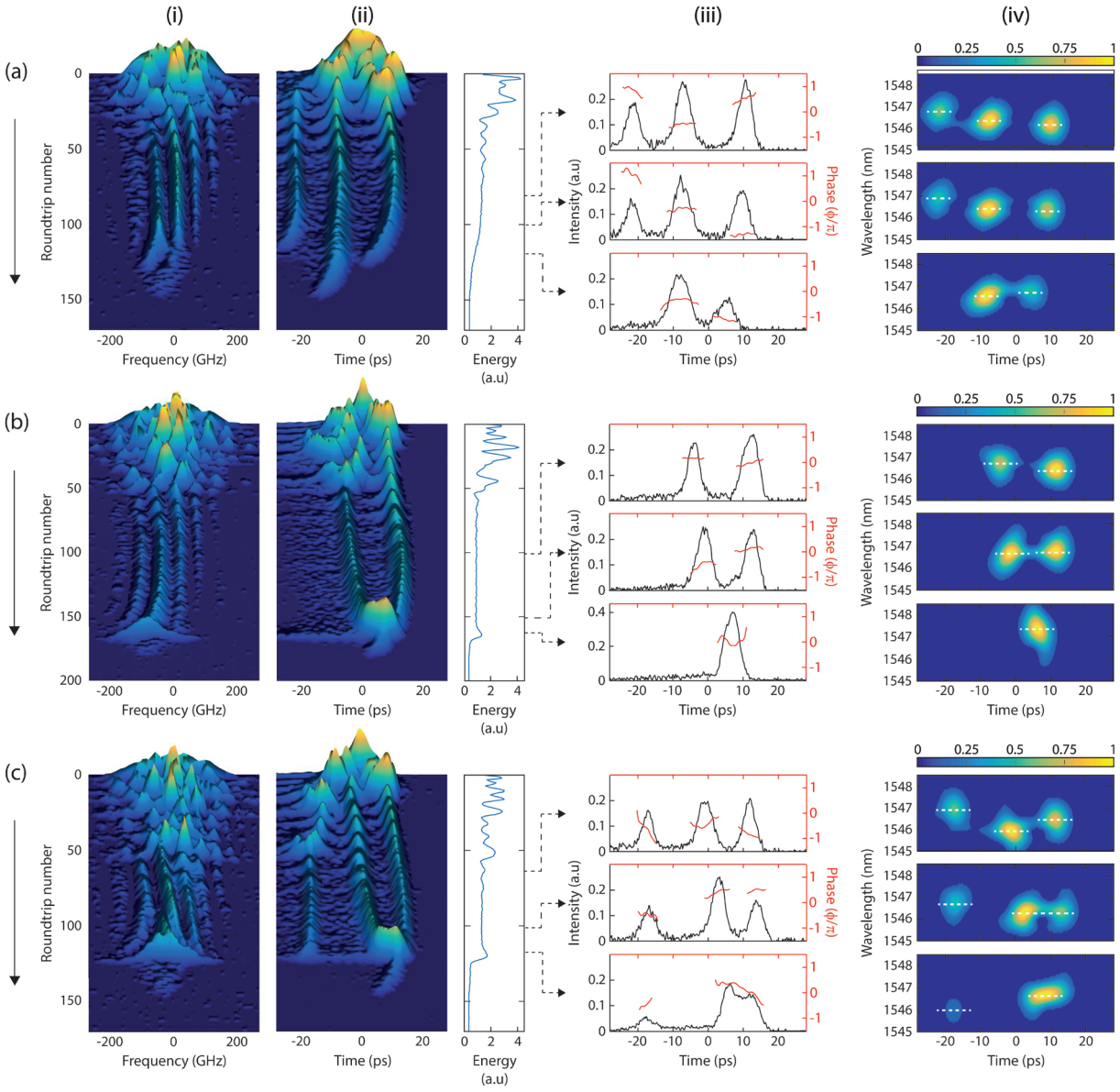

Figure 4. **Real-time spectral and temporal characterization of complex dynamics**. Results showing real-time spectral and temporal characterization for (a) a non-interacting triplet of three solitons over 170 round trips, (b) more complex break-up and collision dynamics of a soliton double pulse over 200 round trips and (c) a combination of a single non-interacting soliton and a two pulse collision over 170 round trips. (i) Measured spectral intensity. (ii) Measured temporal intensity. The right subfigure shows the integrated energy. (iii) Corresponding temporal intensity (left axis) and phase (right axis) extracted using the Gerchberg-Saxton algorithm for pulses at points indicated by arrows. For each of the extracted pulses in (iii), the plots in (iv) show the calculated wavelength-time spectrogram. The dashed line in the spectrogram plots indicate the central frequencies of the coherent pulses and the colour scale shows spectrogram intensity in linear arbitrary units normalised relative to the maximum.

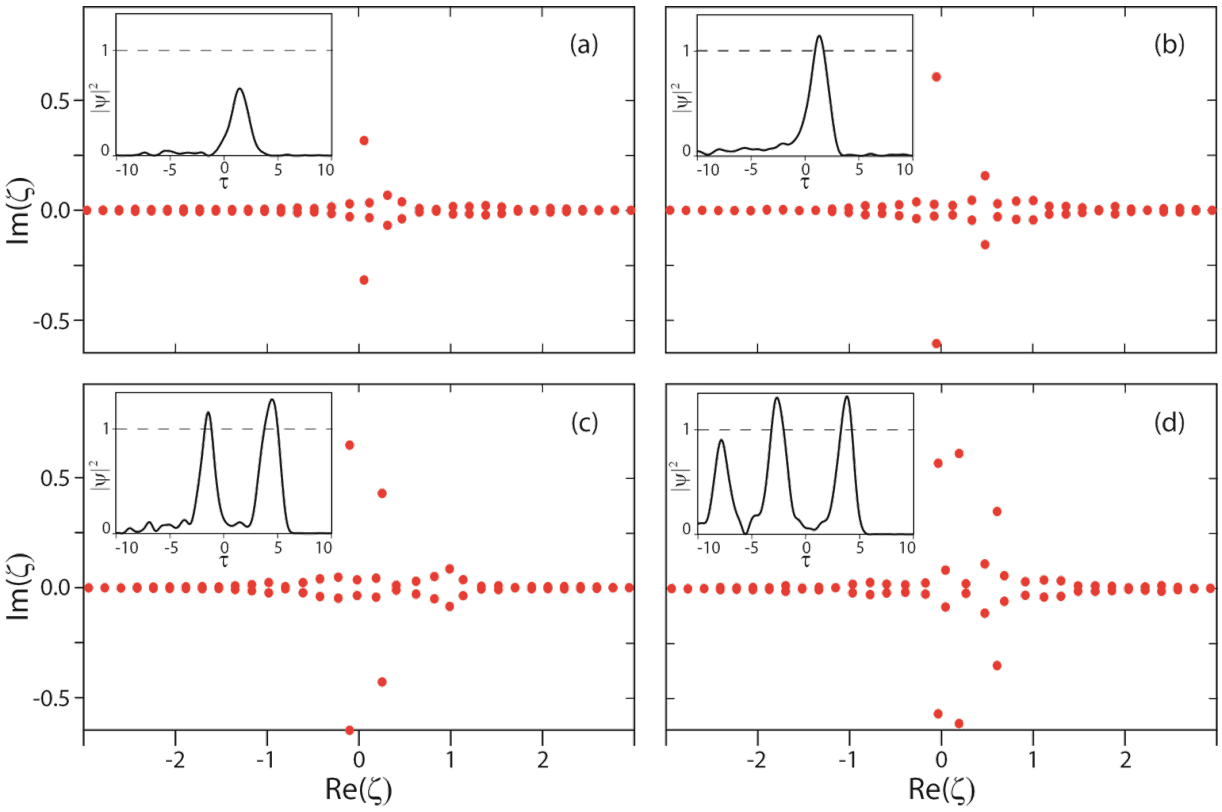

Figure 5. C**alculated eigenvalue content of unstable pulses.** Results applying the scattering transform to intensity and phase measurements of a selection of measured dissipative solitons. In each case the red dots show the calculated discrete eigenspectrum corresponding to the normalized pulse intensity profiles shown as insets. Here ψ is the normalised pulse envelope that generates the scattering potential, τ is the time variable, and ζ is the calculated eigenvalue. The results in Fig 5(a) and (b) correspond to the two points in the dissipative soliton breather cycle shown in Fig. 3(b). As the pulse intensity varies below and above the unity value of a normalized fundamental soliton, the retrieved eigenvalues Im(ζ) varies below and above ±0.5*i*. (c) The double soliton case in Fig. 4(b) where we see two discrete eigenvalues with Im(ζ) ~ ±0.5*i*. (d) The three soliton case in Fig. 4(a) where we see three discrete eigenvalues with Im(ζ) around ±0.5*i*. (Note that the intensity profiles plotted correspond to results shown in Fig. 3 and 4 but have been smoothed for clarity when shown as insets.) The dashed line in the insets shows the intensity of an ideal soliton.